Supporting Information

A Piezo-self-Fenton System Based on Dual Co-catalyst Modified $Bi_4Ti_3O_{12}$ with Accelerated Fe^{3+}/Fe^{2+} Cycle and Efficient In-situ Production of H_2O_2

Yongfei Cui[a,*], Panpan Yuan[a], Wei Liu[a], Zhuo Wang[a], Subhajit Pal[b], Joe Briscoe[b]

[a]School of Materials Science and Engineering, Shaanxi Key Laboratory of Green Preparation and Functionalization for Inorganic Materials, Shaanxi University of Science & Technology, Xi'an 710021 Shaanxi, P. R. China

[b]School of Engineering and Material Science, Queen Mary University of London, Mile End Road, London E1 4NS, United Kingdom

*Corresponding authors: cuiyongfei@sust.edu.cn

Text S1 The iron concentration measured by 1, 10-phenanthroline spectrophotometry

Determination of Fe^{2+} spectrophotometrically by 1,10-phenanthroline [1]: 30 mg of sample powder was added to 30 mL of deionized water containing 10 $mg \cdot L^{-1}$ Fe^{2+}. Ultrasonic excitation was carried out at 50 W, 40 kHz for 10 min, and 2 mL of the reaction solution was taken every 2 min, and then the supernatant was centrifuged. Then 200 μL of the above reaction solution, 1 mL of sodium acetate solution (pH = 4.6), and 200 μL of 1,10-phenanthroline solution (1 $g \cdot L^{-1}$) were taken into a test tube. The volume was fixed to 5 mL by supplementing with deionized water. After 10 min of color development, the absorbance of the resulting substance was measured at 510 nm by a UV-visible spectrophotometer.

Standard curves were obtained by measuring the absorbance of Fe^{2+} solutions at different concentrations to improve the detection accuracy. The results are shown in Fig. S1, and the linearly fitted regression equation of Fe^{2+} solution concentration (x) versus absorbance (y) is shown in equation S1. The test results were substituted into the regression equation of the standard curve to obtain the corresponding Fe^{2+} solution concentration.

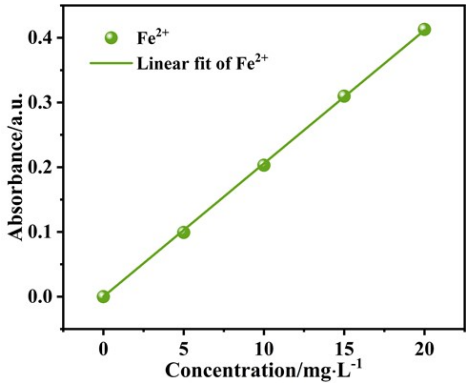

Fig. S1. Standard curve for determination of Fe^{2+} concentration.

$$y = 0.02057x \quad \text{(Equation S1)}$$

Spectrophotometric determination of total iron by 1,10-phenanthroline: the experimental procedure was the same as that for Fe^{2+} determination, except that an additional 200 μL (100 g· L^{-1}) of hydroxylamine hydrochloride (reducing agent) was added. The standard curve was obtained by measuring the absorbance of Fe^{3+} solutions at different concentrations to improve the detection accuracy. The results are shown in Fig. S2, and the linearly fitted regression equation of Fe^{3+} solution concentration (x) versus absorbance (y) is shown in equation S2. The regression equation is close to equation S1, confirming the accuracy of the total iron test method. From this, the concentration of Fe^{3+} can be calculated by equation S3.

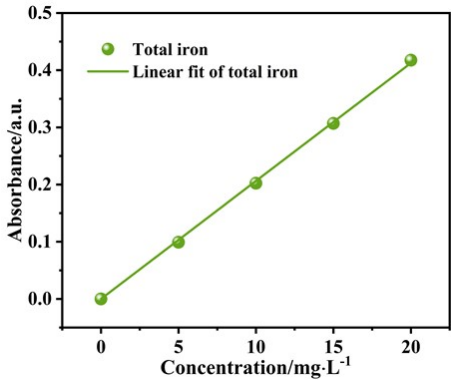

Fig. S2. Standard curve for determination of total iron.

$$y = 0.02063x \quad \text{(Equation S2)}$$

$$C(Fe^{3+}) = C(\text{total iron}) - C(Fe^{2+}) \quad \text{(Equation S3)}$$

Text S4 In situ determination of Fe^{2+} concentration by 1, 10-phenanthroline spectrophotometry [1]

Piezoelectric catalysis experiments were carried out in 1,10-phenanthroline solution using the principle of high reactivity between 1,10-phenanthroline and Fe^{2+}. The conversion of Fe^{2+} to Fe^{3+} by H_2O_2 during catalysis was avoided. In situ detection of Fe^{3+} with 1,10-phenanthroline solution (0.04 g·L^{-1}, pH = 2.5): 30 mg of sample powder was added to 30 mL of 1,10-phenanthroline solution containing 10 mg·L^{-1} Fe^{3+} ($Fe(NO_3)_3·9H_2O$). Ultrasonic excitation was carried out at 50 W, 40 kHz for 20 min, and 2 mL of the reaction solution was taken at 5 min intervals, then the supernatant was separated by centrifugation and the absorbance of the solution was measured by UV-visible spectrophotometer. The test results were substituted into the regression equation S1 to obtain the corresponding Fe^{2+} solution concentration.

Text S3 NBT experiment to determine superoxide radical ($·O_2^-$) concentration

In previous studies, $·O_2^-$ is an important active species in the catalytic process, the nitro tetrazolium blue chloride (NBT) assay is the most typical characterization method [2]. The reaction equation of NBT and $·O_2^-$ is as shown in S4, and the concentration of $·O_2^-$ can be inferred from the consumption of NBT. Detection of $·O_2^-$ with NBT solution (10 mg·L^{-1}): 30 mg of sample powder was added to 30 mL of NBT solution containing 10 mg·L^{-1} Fe^{2+} ($FeSO_4·7H_2O$). After shading and

stirring for 1 h the suspension was excited by sonication at 50 W, 40 kHz. After sonication for 1 h, 3 mL of the reaction solution was taken at 15 min intervals and then centrifuged to separate 2 mL of supernatant, and the absorbance of the NBT solution was measured using a UV-Vis spectrophotometer.

$$NBT + 4 \cdot O_2^- \rightarrow Formazan \quad \text{(Equation S4)}$$

Standard curves were obtained by measuring the absorbance of different concentrations of NBT solutions to improve the detection accuracy. The results are shown in Fig. S3, and the linearly fitted regression equation of NBT solution concentration (x) and absorbance (y) is shown in equation S5. The test results were substituted into the regression equation of the standard curve to obtain the corresponding NBT solution concentration and the concentration of $\cdot O_2^-$ was deduced based on the reaction equation S4.

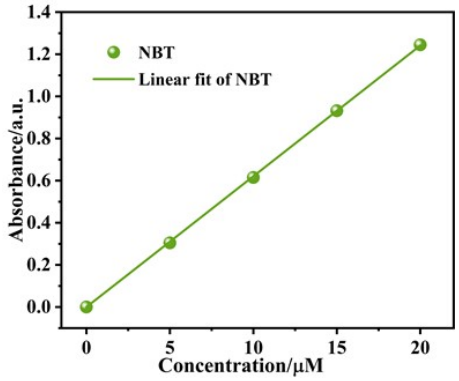

Fig. S3. Standard curve of NBT.

$$y = 0.062x \quad \text{(Equation S5)}$$

Text S2 Coumarin determination of hydroxyl radical (·OH) concentration

The presence and role of the Fenton process can be visualized by determining the concentration of ·OH produced. In this paper, coumarin was used as a probe molecule and the reaction equation is shown in S6, which produces 7-hydroxycoumarin by the reaction of coumarin with ·OH [3,4]. 7-Hydroxycoumarin is a strongly fluorescent substance and the concentration of ·OH can be obtained by measuring the fluorescence intensity of 7-hydroxycoumarin. Detection of ·OH was performed with coumarin solution (1 mM): 30 mg of sample powder was added to 30 mL of coumarin solution containing 10 $mg \cdot L^{-1}$ Fe^{2+} ($FeSO_4 \cdot 7H_2O$). After shading and stirring for 1 h the suspension was excited by sonication at 50 W, 40 kHz. After 1 hour of sonication, 3 mL of the reaction solution was taken at 15-minute intervals and then centrifuged to remove the powder, and the fluorescence intensity of the 7-hydroxycoumarin solution was measured by a fluorescence spectrophotometer.

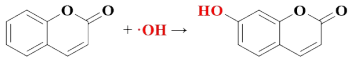

(Equation S6)

The standard curve was obtained by measuring the fluorescence intensity of 7-

hydroxycoumarin solution at different concentrations to improve the detection accuracy. The results are shown in Fig. S4, and the regression equation of linear fitting of 7-hydroxycoumarin solution concentration (x) and fluorescence intensity (y) is shown in equation S7. The test results were substituted into the regression equation of the standard curve to obtain the corresponding 7-hydroxycoumarin solution concentration. The concentration of ·OH was deduced based on the reaction equation S7.

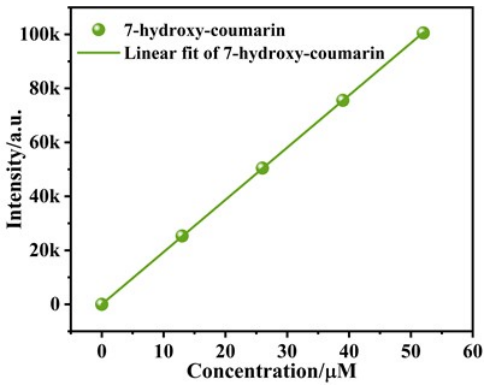

Fig. S4. Standard curve of 7-hydroxycoumarin.

$$y = 1935.8x \quad \text{(Equation S7)}$$

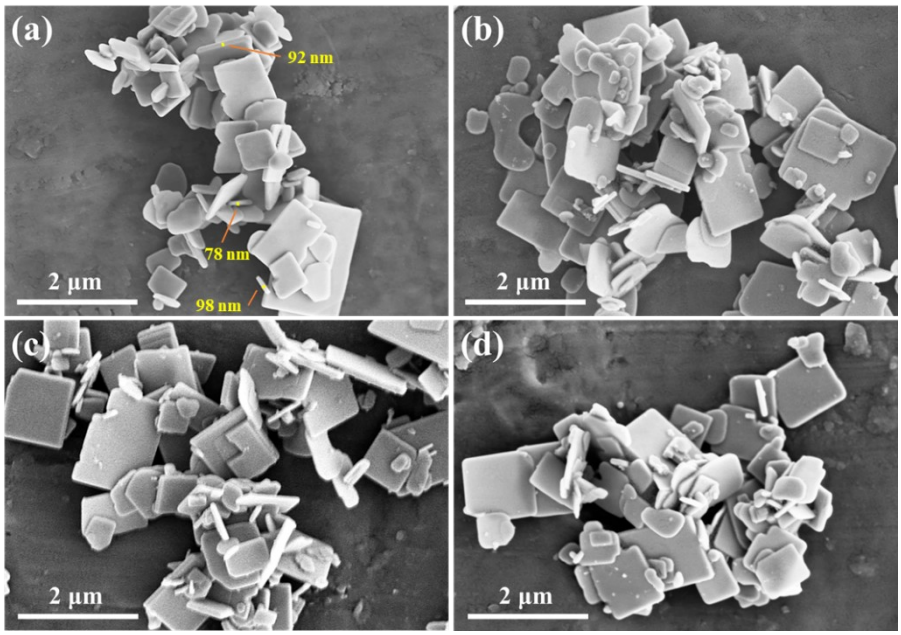

Fig. S5. SEM images of (a) BTO, (b) Ag/BTO/CoO_x-1, (c) Ag/BTO/CoO_x-2 and (d) Ag/BTO/CoO_x-3.

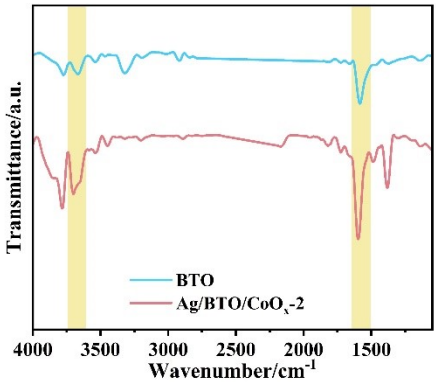

Fig. S6. FT-IR spectra of Ag/BTO/CoO_x-2 and BTO.

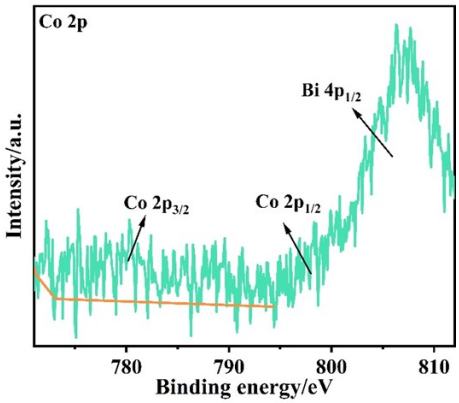

Fig. S7. Test data from high-resolution XPS spectra of Co 2p.

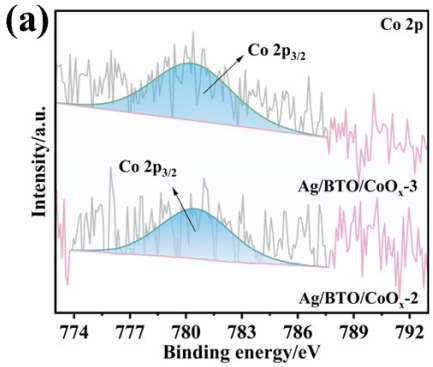

(b)

Catalyst \ at./%	Ag	Co
Ag/BTO/CoO_x-2	0.54	0.05
Ag/BTO/CoO_x-3	0.74	0.11

Fig. S8. (a) The high-resolution XPS spectra of Co 2p and (b) Ag and Co atomic ratio in Ag/BTO/CoO_x-3 and Ag/BTO/CoO_x-2.

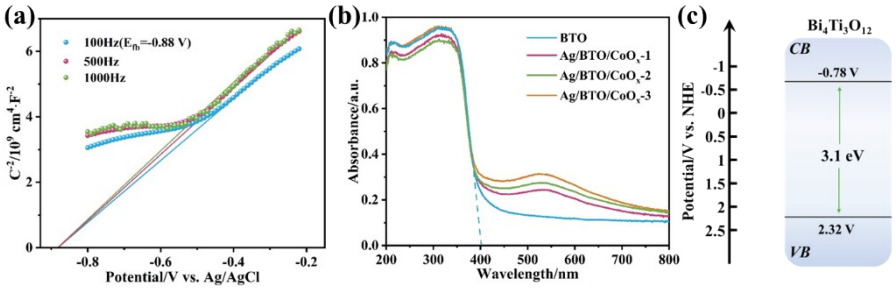

Fig. S9. (a) Mott-Schottky curve of BTO, (b) UV-Vis diffuse reflectance spectra and (c) schematic diagram of BTO energy band structure.

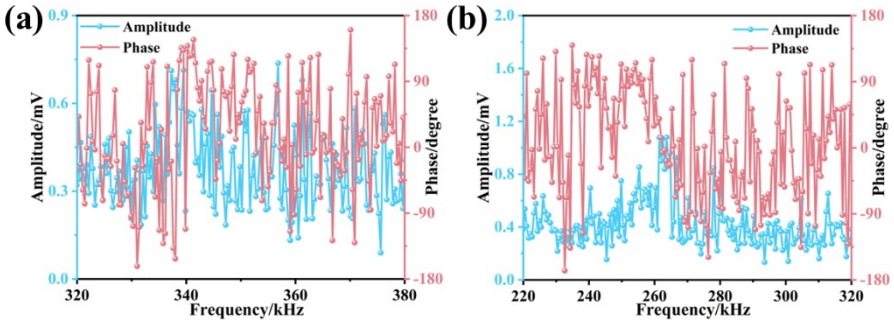

Fig. S10. Phase and amplitude sweep on the substrate of (a) BTO and (b) Ag/BTO/CoOx-2.

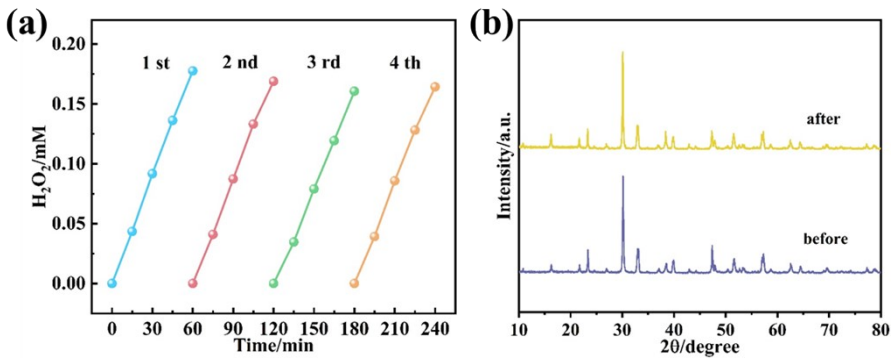

Fig. S11. (a) cycle experiment of the piezoelectric catalyzed generation of H_2O_2 with Ag/BTO/CoO_x-2 and (b) XRD patterns of the samples before and after cycle tests.

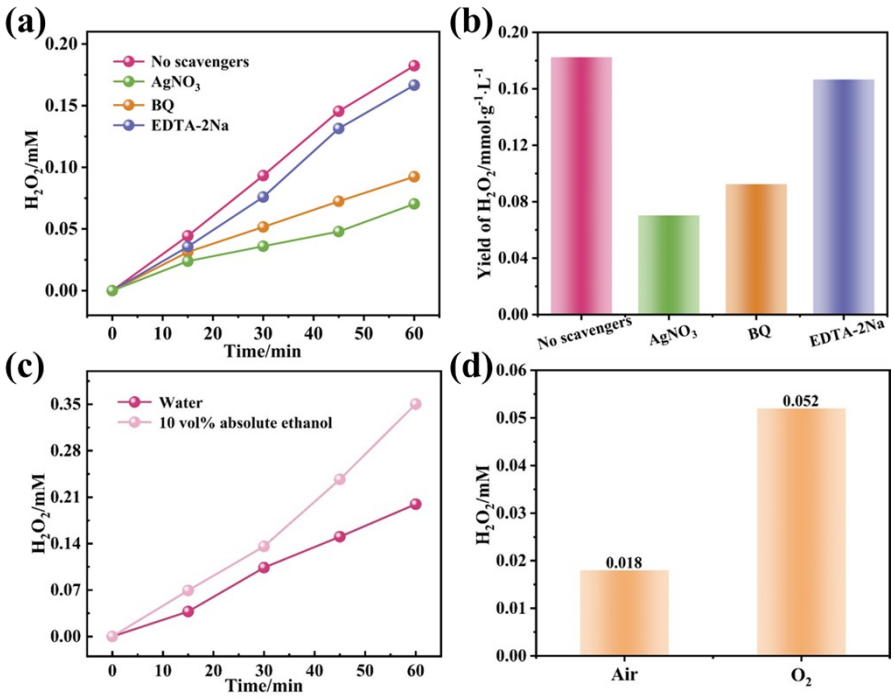

Fig. S12. Piezocatalytic generation of H_2O_2 with Ag/BTO/CoO_x-2 (a) capture experiment, (b) H_2O_2 yield, piezo-catalysed H_2O_2 production from Ag/BTO/CoO_x-2 samples in (c) different solvents and (d) different atmospheres.

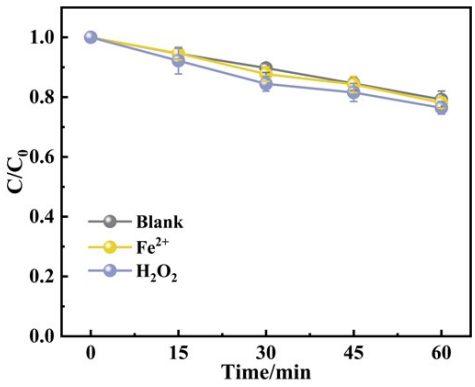

Fig. S13. Piezo-self-Fenton degradation of RhB.

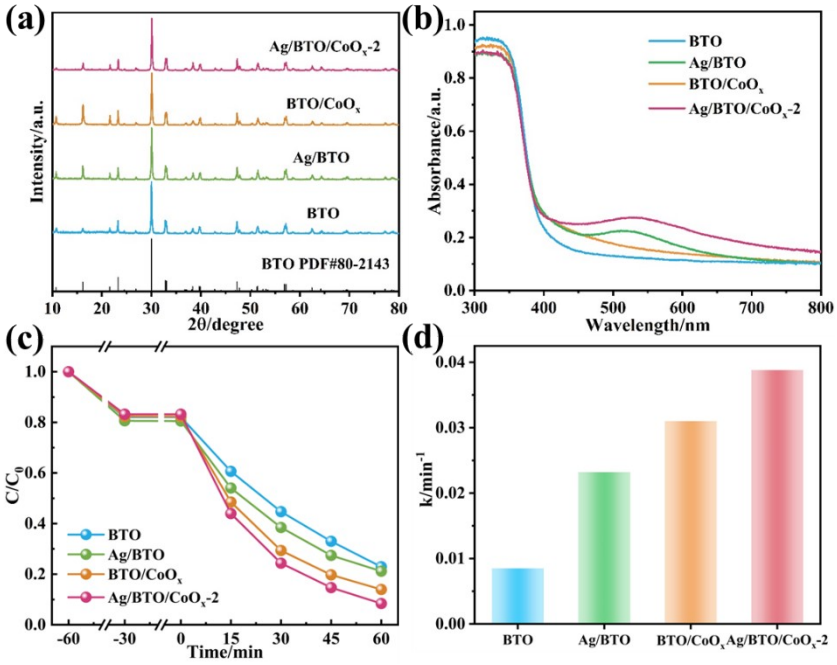

Fig. S14. (a) XRD patterns, (b) UV-Vis diffuse reflectance spectra, (c) piezo-self-Fenton-degradation curves of RhB and (d) first-order reaction rate constant of single cocatalyst modified BTO.

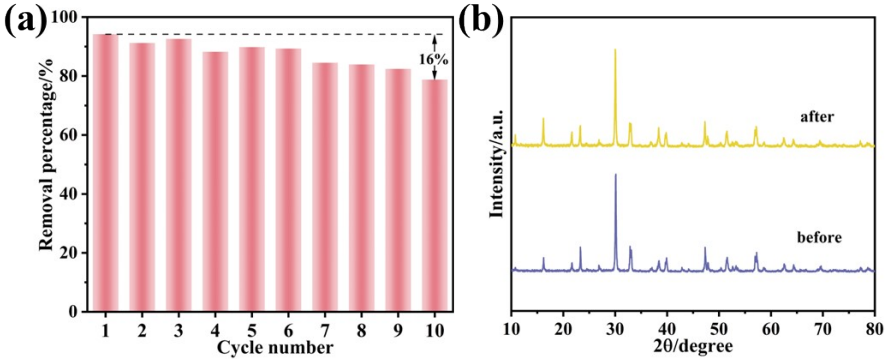

Fig. S15. (a) Piezo-self-Fenton degradation cycling experiment of RhB by Ag/BTO/CoO_x-2 samples and (b) XRD patterns of samples before and after cycling.

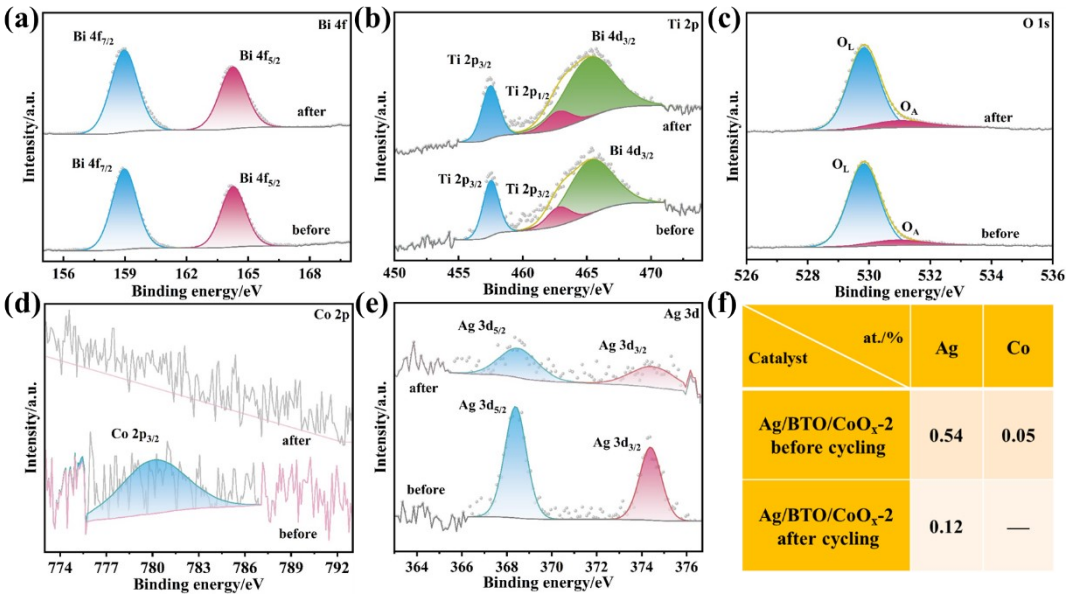

Fig. S16. The high-resolution XPS spectra of (a) Bi 4f, (b) Ti 2p, (c) O 1s, (d) Co 2p, (e) Ag 3d and (f) atomic ratio of Ag and Co in Ag/BTO/CoO_x-2 before and after cycling.

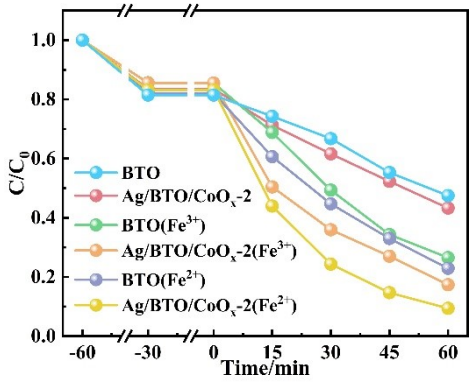

Fig. S17. Degradation curves of RhB in the presence of Fe^{2+} (10 mg·L^{-1}) or Fe^{3+} (10 mg·L^{-1}).

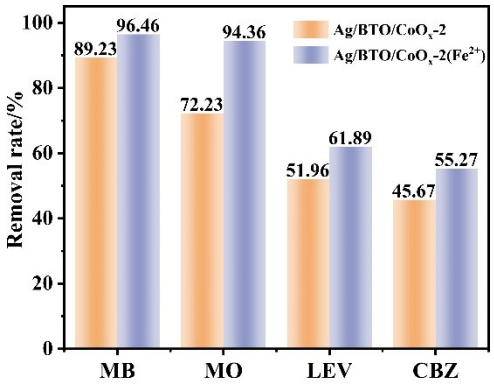

Fig. S18. Degradation rates of several common organic pollutants.

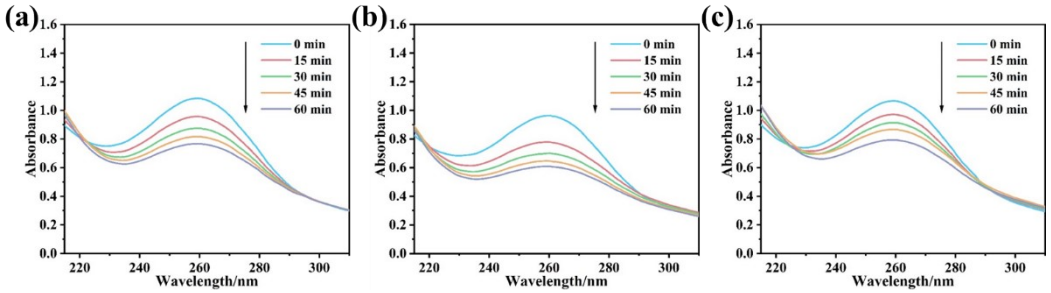

Fig. S19. UV-vis absorption spectra of NBT under different conditions (a) Ag/BTO/CoO_x-2, (b) BTO (Fe^{2+}) and (c) BTO.

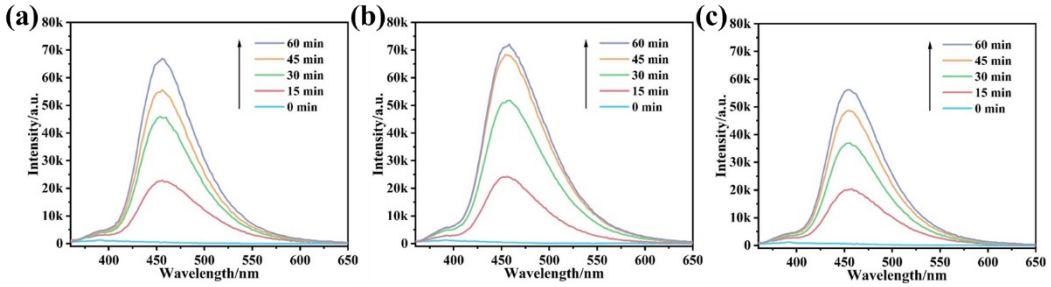

Fig. S20. Fluorescence spectra of 7-hydroxycoumarin (a) Ag/BTO/CoO_x-2, (b) BTO (Fe^{2+}) and (c) BTO.

Table S1. Chemical composition results obtained by XRF.

Catalyst	Ag (*at.*/%)	Co (*at.*/%)	Bi (*at.*/%)	Ti (*at.*/%)
Ag/BTO/CoO_x-3	0.12	0.19	64.47	35.22
Ag/BTO/CoO_x-2	0.09	0.10	64.4	35.41
Ag/BTO/CoO_x-1	0.08	0.04	63.88	36
Ag/BTO/CoO_x-2 after cycling	0.04	0.03	64.26	35.67

Table S2. Comparison of the experimental parameters between Ag/BTO/CoO_x and the reported literatures.

Catalyst	Ultrasound parameter	Dosage	Yield of H_2O_2 /mmol·g^{-1}·h^{-1}	Organic contaminants/ piezo-Fenton degradation efficiency	Ref.
Ag/BTO/CoO_x	40 kHz, 50 W	30 mg/ 30 mL	0.17	10 ppm, RhB/ 85% in 40 min 10 ppm, MB/ 93% in 15 min 10 ppm, MO/ 89% in 40 min	this work
ZnS/In_2S_3/$BaTiO_3$	40 kHz, 150 W	10 mg/ 50 mL	0.11	——	5
$RbBiNb_2O_7$	68 kHz, 260 W	20 mg/ 30 mL	0.02	——	6
$BaTiO_3$	80 kHz, 50 W	50 mg/ 50 mL	0.06	10 ppm, RhB/ 69.7% in 40 min 10 ppm, MB/ 42% in 15 min 10 ppm, MO/ 43.1% in 40 min	7
Fe_3O_4-$BaTiO_3$	40 kHz, 150 W	50 mg/ 50 mL	——	5 ppm, RhB/ 46% in 40 min	8
$CoFe_2O_4$@ ZnS	37 kHz, 100 W	25 mg/ 50 mL	——	25 ppm, RhB/ 48% in 40 min 25 ppm, MB/ 34% in 15 min 25 ppm, MO/ 37% in 40 min	9
g-C_3N_4-Fe	40 kHz, 300 W	100 mg/ 100 mL	0.166	10 ppm, MB/ 81% in 15 min	10

Reference

1 J. Xu, Q. Zhang, X. Gao, P. Wang, H. Che, C. Tang and Y. Ao, *Angew. Chem. Int. Ed.*, 2023, **62**, e202307018.

2 Y. Cui, P. Yuan, F. Wang, W. Liu, Z. Wang, X. Tao, J. Briscoe and Y. Pu, *J. Alloys Compd.*, 2024, **980**, 173671.

3 Y. Wu, P. Wang, H. Che, W. Liu, C. Tang and Y. Ao, *Angew. Chem. Int. Ed.*, 2024, **63**, e202316410.

4 S. Chen and H. Lei, *Tribol. Int.*, 2024, **194**, 109549.

5 X. Zhou, B. Shen, J. Zhai and J. C. Conesa, *Small Methods*, 2021, **5**, 2100269.

6 Y. Ma, B. Wang, Y. Zhong, Z. Gao, H. Song, Y. Zeng, X. Wang, F. Huang, M.-R. Li and M. Wang, *Chem. Eng. J.*, 2022, **446**, 136958.

7 H. Gao, Y. Zhang, H. Xia, X. Mao, X. Zhu, S. Miao, M. Shi and S. Zha, *Dalton Trans.*, 2022, **51**, 11876–11883.

8 J. Xie, Q. Liu, L. Huang, X. Chen, C. Zhao, X. Wu, T. Lin, Y. Wu, M. Gao and C. Lin, *Chem. Eng. J.*, 2024, **487**, 150685.

9 S. Farhadi, F. Siadatnasab and A. Khataee, *Ultrason. Sonochem.*, 2017, **37**, 298–309.

10 L. Ge, J. Xiao, W. Liu, G. Ren, C. Zhou, J. Liu, J. Zou and Z. Yang, *Chem. – Eur. J.*, 2022, **28**, e202202494.